

Model and Control of Tendon-Sheath Transmission Systems

G. Palli and C. Melchiorri

*DEIS, Dept. of Electronics, Computer Science and Systems
University of Bologna
Via Risorgimento 2, 40136 Bologna, Italy
{gpalli, cmelchiorri}@deis.unibo.it*

Abstract— In this paper, the tendon-sheath driving system for a robotic hand is presented and its force transmission characteristics are analyzed. The use of tendon-based transmission permits to reduce the size and the complexity of the actuation chain in many mechanical devices. A simple static model that describes the tendon-sheath driving system is presented, and its behavior is compared both with simulative results, obtained with a lumped parameters model of the tendon, and with experimental results. Different static and dynamic friction models are used in the simulations and the related results are compared to highlight some phenomena that are not visible from the static model of the tendon. A simple force control algorithm with feedforward friction compensation based on the static friction model is also presented.

Index Terms— Tendon-sheath transmission, friction compensation, force control, impedance control, robotic hand.

I. INTRODUCTION

Tendon-sheath transmission systems are used in various robotic applications, such as robotic hands [1], [2], because very often it is not possible to place the actuators inside the fingers. The use of pulleys increases the mechanical complexity and the dimension of the structure and implies that the tendons must be properly preloaded, while the use of sheaths reduces the size, the complexity, the cost and at the same time increases the reliability of the overall system.



Fig. 1. In the UBHand III the hinges are constituted by flexible sheaths.

This transmission modality introduces some side effects due to the tendon compliance and to the friction between tendon and sheath. These phenomena introduce deadzone, hysteresis and direction-dependent behavior in the force control [6].

A simple tendon-sheath static model that highlight nonlinearities and direction-dependent behavior is presented in [6], [7]. Starting from this model, we have made some additional

considerations about environment disturbance and tension distribution along the tendon. The environment is modeled as a mass linked to a mobile constrain by a spring. The disturbance is represented by the movement of the constrain and by an external force applied to the environment mass. This model is adequately modified to consider the effect of non-constant preload and environment disturbance.

In [7], a lumped parameters dynamical model is used to validate the input-output relation derived from the experiments. We use a similar model in simulation to study the tension distribution inside the tendon and the effect of the environment load. In our work, we show that this model has a strange behavior in stationary condition due to the considered static friction model (Coulomb friction). The use of a dynamical friction model (Dahl model [8]) corrects this drawback.

In order to compensate the nonlinear behavior of the driving system, a suitable controller with a friction compensator is designed. The friction compensation law presents discontinuities when the sign of the tendon velocity changes, so the bandwidth of the actuators must be very high to obtain good performance. This switching control action introduces dynamics behaviors in the system, such as vibrations in the tendon, that are not considered in the static tendon model. Simulative results show that this controller is able to compensate both friction effects and also the environment disturbances.

II. TRANSMISSION CHARACTERISTICS

The static model of the tendon-sheath driving system presented in [6], [7] is (see Fig. 2):

$$\begin{aligned} F_f &= \mu N \text{sign}(\dot{\epsilon}) \\ \Delta T &= -F_f \\ \delta &= \frac{1}{EA} T = \rho T \end{aligned}$$

where E , A , and δ are respectively the Young modulus, the cross sectional area and the elongation of the tendon, $\dot{\epsilon}$ and T are the tendon velocity and tension, F_f and N are the friction force and the normal load acting between the tendon and the sheath respectively, and

$$\mu = \begin{cases} \mu_s & \text{if } \dot{\epsilon} = 0 \\ \mu_d & \text{if } \dot{\epsilon} \neq 0 \end{cases}$$

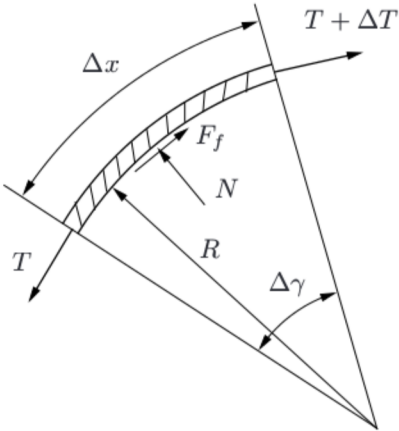


Fig. 2. Equilibrium of a tendon element.

is the Coulomb friction coefficient. Assuming that $\dot{\epsilon}$ has the same sign along the whole length of the tendon, and neglecting the effect of stiction, we can model an infinitesimal tendon element as:

$$N = T d\gamma = T \frac{dx}{R} \quad (1)$$

$$dT = -F_f = -\mu T \frac{dx}{R} \text{sign}(\dot{\epsilon}) \quad (2)$$

where $d\gamma$ is the angle subtended by the arc of length dx and R is the radius of the sheath curvature. From these equations we can write:

$$\begin{bmatrix} \frac{dT}{dx} \\ \frac{d\delta}{dx} \end{bmatrix} = \begin{bmatrix} -\frac{\mu}{R} \text{sign}(\dot{\epsilon}) & 0 \\ \frac{1}{EA} & 0 \end{bmatrix} \begin{bmatrix} T \\ \delta \end{bmatrix} + \begin{bmatrix} 0 \\ -\frac{1}{EA} \end{bmatrix} T_0$$

or, in more compact form

$$\frac{d\theta}{dx} = D\theta + \Lambda T_0 \quad (3)$$

where T_0 is the tendon preload. The solution of this system is:

$$T(x) = \begin{cases} T_{in} \exp\left[-\frac{\mu}{R}x \text{sign}(\dot{\epsilon})\right] & \text{if } x < L_1 \\ T_0 & \text{if } x \geq L_1 \end{cases} \quad (4)$$

$$\delta(x) = \begin{cases} \left[H(x) - T_0 x + \frac{R}{\mu} T_{in} \text{sign}(\dot{\epsilon})\right] \rho & \text{if } x < L_1 \\ \left[H(L_1) - T_0 L_1 + \frac{R}{\mu} T_{in} \text{sign}(\dot{\epsilon})\right] \rho & \text{if } x \geq L_1 \end{cases} \quad (5)$$

where

$$H(x) = -\frac{R}{\mu} T_{in} \text{sign}(\dot{\epsilon}) \exp\left[-\frac{\mu}{R} x \text{sign}(\dot{\epsilon})\right] \quad (6)$$

and

$$L_1 = \min\{x \in T(x) = T_0\}$$

When L_1 becomes equal to L , to variation of the input tension is immediately transmitted to the output side, with a ratio of:

$$\frac{dT_{out}}{dT_{in}} = e^{-v} \quad \text{if } \dot{\epsilon} > 0$$

$$\frac{dT_{out}}{dT_{in}} = e^v \quad \text{if } \dot{\epsilon} < 0$$

where

$$v = \frac{\mu}{R} L$$

This implies that $\dot{\epsilon}$ has the same sign along the tendon, positive during the pulling phase and negative during the loosening one.

This model is obtained by considering only the static Coulomb friction. With a dynamical friction model, in our case the Dahl model (see Fig. 3), it is possible to see that the slope of the exponential term of the (4) can assume all the intermediate values between v and $-v$. To explain this phenomenon, we can note that in (2), the variation of the tendon tension is due only to the Coulomb friction. In the Dahl model, the value of friction can vary between F_c and $-F_c$, where F_c is the absolute value of the Coulomb friction.

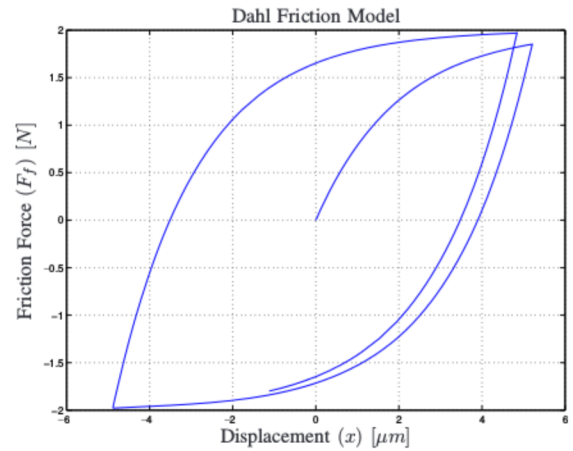


Fig. 3. The Dahl friction model.

III. TENDON DYNAMICAL MODEL

A lumped parameters tendon model similar to the one presented in [7] is used for simulation. The equilibrium of

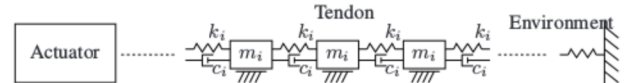


Fig. 4. Lumped parameter tendon model.

each tendon element is given by:

$$m_i \ddot{\epsilon}_i - c_i (\dot{\epsilon}_{i+1} - 2\dot{\epsilon}_i + \dot{\epsilon}_{i-1}) = T_i^+ + T_i^- - F_{fi} \quad (7)$$

$$T_i^+ + T_i^- = k_i (\epsilon_{i+1} - 2\epsilon_i + \epsilon_{i-1}) \quad (8)$$

$$\begin{aligned} F_{fi} &= \frac{\mu}{2R} (T_i^+ - T_i^-) \tanh(k_v \dot{\epsilon}_i) = \\ &= \frac{\mu}{2R} k_i (\epsilon_{i+1} - \epsilon_{i-1}) \tanh(k_v \dot{\epsilon}_i) \end{aligned} \quad (9)$$

where m_i , ϵ_i , c_i , F_{fi} , T_i^+ , T_i^- , k_v and k_i are respectively the mass, the position, the damping, the friction, the input side

tension, the output side tension, the friction parameter in the Karnopp model and the stiffness of each tendon element (see Fig. 4).

Note that the $\text{sign}(\cdot)$ function in the Coulomb friction model is replaced in the Karnopp model by the $\tanh(\cdot)$ function, eq. (9), to avoid numerical problems during simulation [8].

The simulation results highlight that in stationary conditions the tendon tension distribution shows a behavior without physical meaning, see Fig. 5. In particular, it is possible to note that the output tension increases without an input tension variation, as if the effect of friction is vanishing. This fact

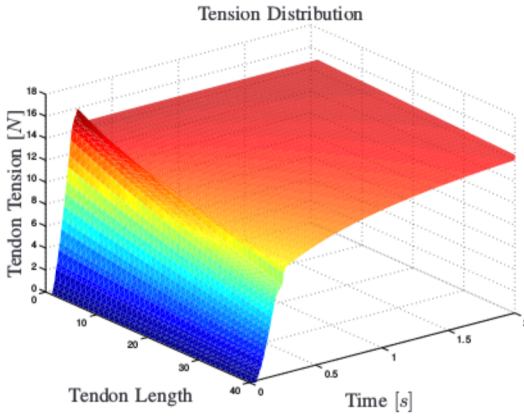


Fig. 5. Simulation results: tendon tension distribution.

is due to the friction model used, that neglects the stiction effect. The use of the Dahl friction model [8] permits to take into account the effects of the friction also when the velocity goes to zero and for little movements. Now, the equilibrium of each tendon element is given by:

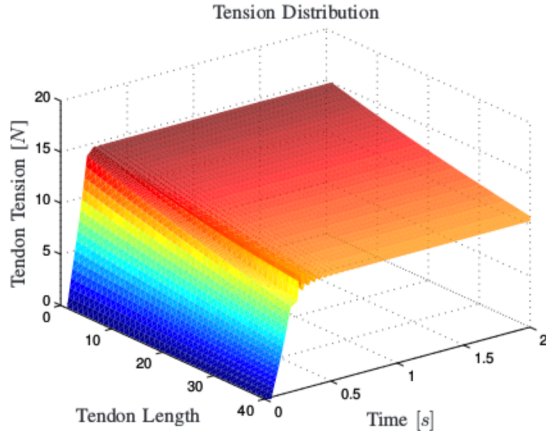


Fig. 6. Simulation results: tendon tension distribution.

$$\dot{\epsilon}_i = v_i \quad (10)$$

$$\dot{v}_i = \frac{1}{m_i} [c_i(v_{i+1} - 2v_i + v_{i-1}) + k_i(\epsilon_{i+1} - 2\epsilon_i + \epsilon_{i-1}) - F_{fi}] \quad (11)$$

$$\dot{F}_{ai} = k_b \left[v_i - \frac{2nR F_{fi} |v_i|}{\mu L k_i(\epsilon_{i+1} - \epsilon_{i-1})} \right] \quad (12)$$

where k_b is the bristle stiffness characterizing the contact between tendon and sheath.

With this model, also the friction force F_{fi} is a state variable. The equation (12) is the Dahl friction derivative for the considered system. The parameter n (the number of tendon elements) has been set to 40 to reduce the simulation time and the results granularity. The considered tendon length is 0.1[m].

The choice of the this friction model is justified also by the simulation results, as it is possible to see in Fig. 6.

Other dynamic friction models could be evaluated (e.g. LuGre model, Bliman and Sorine model etc. [8]) but an adequate parameters identification procedure is necessary to apply more sophisticated models.

The transmission characteristic obtained from simulations is reported in Fig. 7. In this plot, we can recognize four

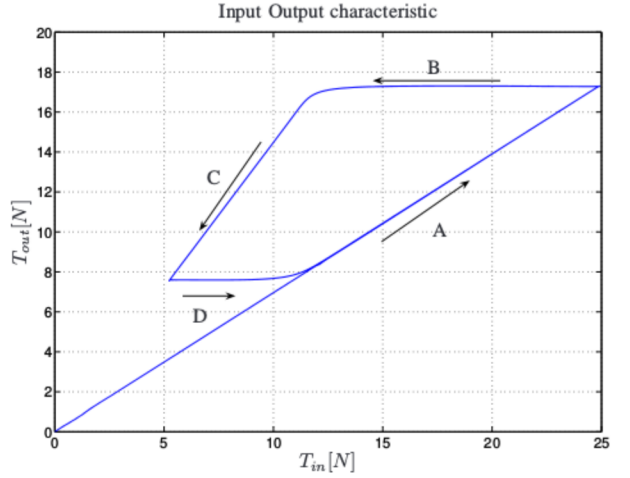


Fig. 7. Simulation results: tendon tension input-output characteristic.

phases: pulling phase (A), relaxation dead zone (B), loosening phase (C) and stretching dead zone (D).

Figure 8 shows the distribution of tension along the tendon when a sinusoidal input is applied.

IV. EXPERIMENTAL RESULTS

In order to validate the simulation results and also to characterize the friction parameters of different materials, for both tendon and sheath (alloy-alloy, Kevlar-alloy, Teflon-alloy, Teflon-Teflon, spectra-alloy, spectra-Teflon), some experiments have been conducted. In the laboratory setup, the tendon is connected at each end to an actuator, composed by a DC motor with encoder, gearheads and ballskrew. The input and output tensions are measured by two load cells,

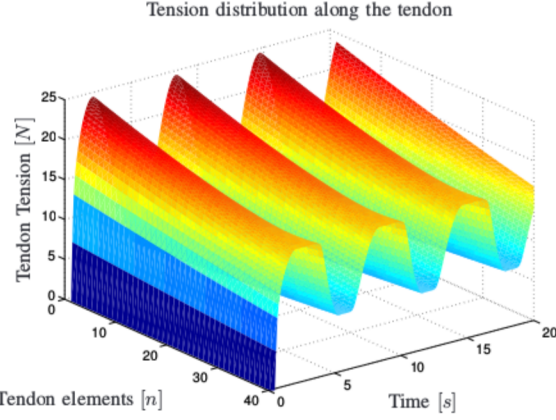


Fig. 8. Simulation results: tendon tension distribution in the dynamic model with sinusoidal input.

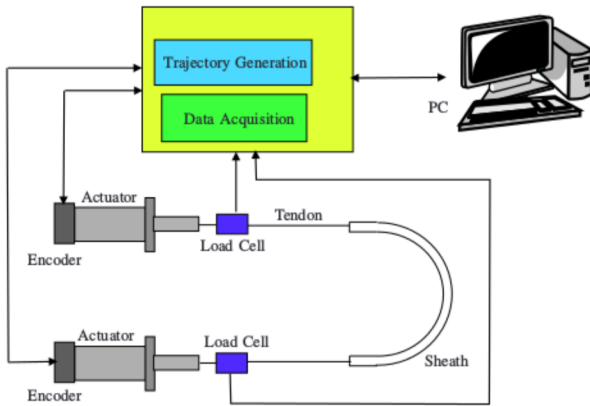


Fig. 9. Acquisition system.

placed at each tendon end. The sheath curvature radius R can be changed, replacing the black plastic cylinder visible in Fig. 10, and the possible bending angles γ are $\pi/2$, π and $3\pi/2$.

The experimental results in Fig. 11(a) and Fig. 11(b) confirm that the transmission characteristic (alloy-alloy) does not depend on the tendon length, but only on the bending angle γ . The parameters of friction can be determined from the transmission characteristic (see Fig. 12(a)). The comparison between simulation and experimental results (see Fig. 12(b)) validates the proposed model.

From Fig. 12(b) it is also possible to note that for high tendon tension, the compliance of the sheath is not negligible. A model that takes into account also the elasticity and the dynamics of the sheath is under development.

V. TENDON TRANSMISSION CONTROL

The main target of this research is to control the output tension of the tendon compensating friction and elasticity effects, and avoiding some typical side effects like limit cycles [9], [10], that classic PID controller introduces in

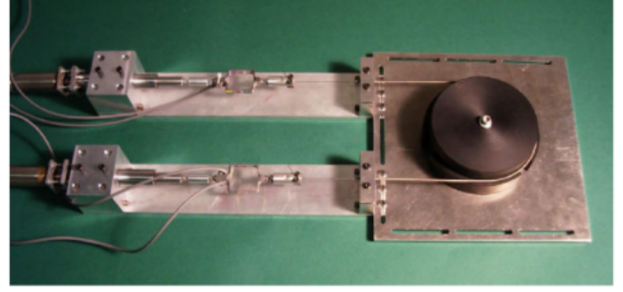


Fig. 10. Experimental setup.

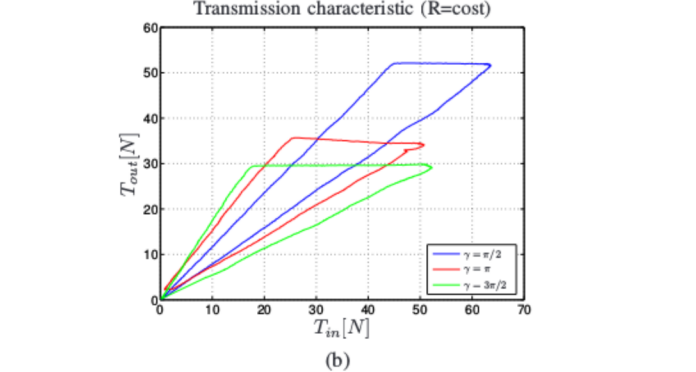
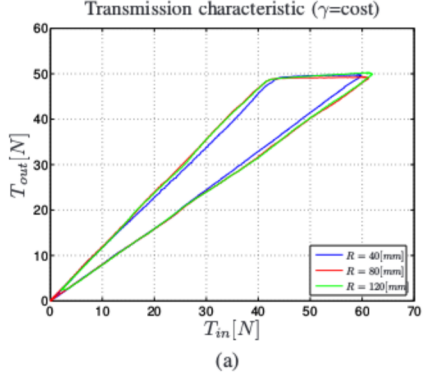


Fig. 11. Experiment results: transmission characteristic from constant bending angle (a) and constant tendon length (b).

this kind of nonlinear systems. For this purpose, a friction compensator is designed so that a suitable action is added to the input tension in order to obtain the desired value for the output tension, eq. (4).

The friction compensation law is not based on the tendon velocity, but on the tension tracking error because if the environment constraint is considered fix, a positive tracking error means that the tendon must be pulled and then the tendon velocity must become positive and vice versa. So the control action F_c is:

$$F_c = T_s \exp \left[\frac{\mu_d}{R} L \operatorname{sign}(e) \right] \quad (13)$$

where T_s is the tension setpoint and e is the tension tracking error.

In Fig. 13(a) the response of the tension control system is

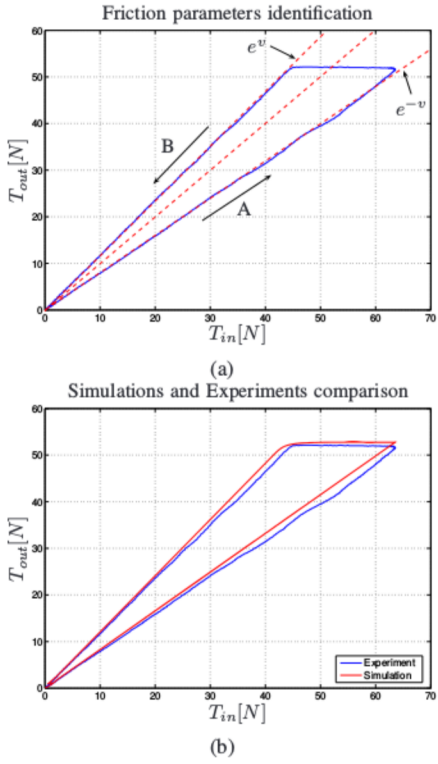


Fig. 12. Experimental results: identification of friction parameters (a) and comparison between simulation and experimental results (b).

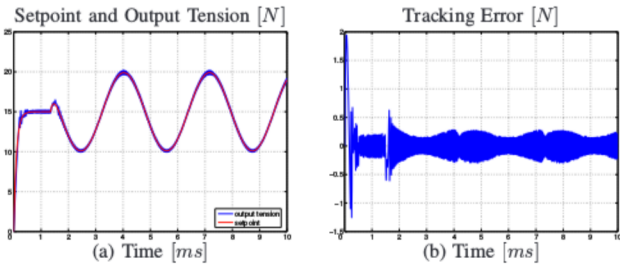


Fig. 13. Setpoint, tendon output tension (a) and tracking error (b).

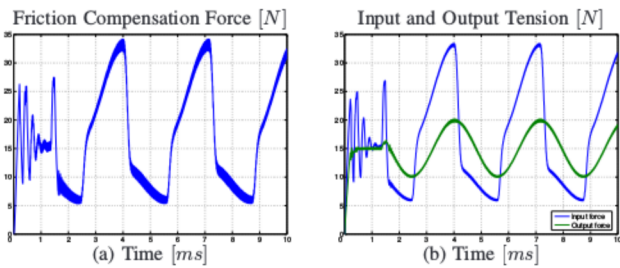


Fig. 14. Input tension from friction compensator (a), input and output tendon tension (b).

reported. In Fig.13(b) it is possible to see that the tracking error is very small also with sinusoidal setpoint, but presents fast variations due to the switching behavior of the friction compensation action (see also Fig.14(a)). In Fig. 14(b) the tendon input and output tensions are reported.

The friction compensation law described by eq.(13) is very similar to a sliding mode controller, because the control action switches from a maximum to a minimum value related to the magnitude of the disturbance (friction). Note that in eq.(13) if the parameters R and L are constant the exponential term may be computed only once both for positive and negative tracking error.

In order to reduce the error chattering, a proper boundary layer is introduced. The new friction compensation action is:

$$F_c = \begin{cases} T_s \exp \left[\frac{\mu_d}{R} L \operatorname{sign}(e) \right] & \text{if } |e| \geq e_{th} \\ T_s \left(1 + \frac{|e|}{e_{th}} \exp \left[\frac{\mu_d}{R} L \operatorname{sign}(e) \right] \right) & \text{if } |e| < e_{th} \end{cases} \quad (14)$$

where e_{th} is the amplitude of the boundary layer.

The response of this controller is reported in Fig. 15(a) and Fig. 15(b). From these Figures it is possible to note that the boundary layer makes the tracking error much more smooth for fixed setpoint, see Fig.15(b) from $t = 0$ to $t = 2$. For $t > 2$ a variation on the environment disturbance is introduced, and this causes a significative growth of the tracking error.

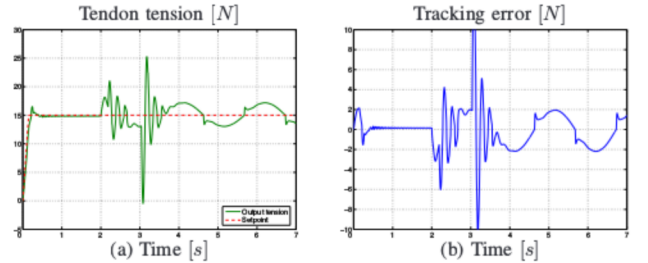


Fig. 15. Setpoint, output tension (a) and tracking error (b) with the boundary layer.

By a suitable overestimation of the friction parameter, it is also possible to compensate for the effects of an environment disturbance. This is done by increasing the magnitude of the control action computed in eq.(14) with a suitable choice of the friction coefficient μ_d . Fig.16(a) and Fig.16(b) report the response and the tracking error with a sinusoidal setpoint starting at time $t = 4.8s$ and a sinusoidal environment constrain motion.

VI. CONCLUSIONS AND FUTURE WORK

In this paper, static and dynamic model of the tendon-sheath driving system are presented. A tendon tension sliding mode controller for the friction compensation is applied to this transmission system and some simulation results are reported. These results show that the output tension of the tendon can be controlled with a limited tracking error even in presence of environment disturbance and without introducing any limit cycle.

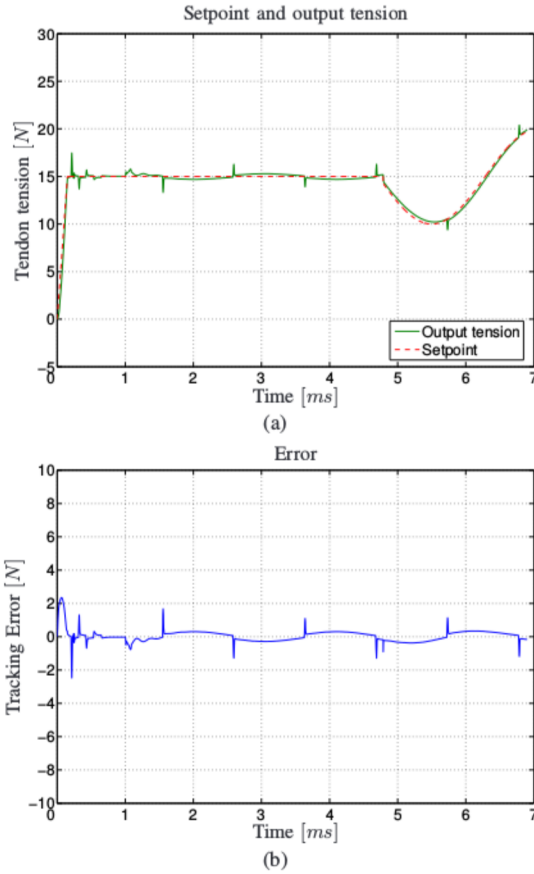


Fig. 16. Setpoint, output tension (a) and tracking error (b) with the overestimation of the disturbance.

The experiments on the tendon-sheath driving system is not concluded yet: in particular the control algorithm has not been tested on the experimental setup. In order to improve the reliability of the simulations and to take into account various friction phenomena, a more complex dynamic friction model may be considered, i.e. the LuGre model.

In a tendon-sheath driving system, a fundamental rule is played by the sheath, whose dynamics is neglected at the moment. A simple model of the sheath that takes into account its finite stiffness is under development.

The dynamics of the nonconstrained parts of the sheath is very important because the mass of the sheath is many times larger than the mass of the tendon, and this may affect the force transmission properties of the system. A tendon-sheath PDE model is under development. Starting from this model it will be possible to use the infinite dimension port-Hamiltonian approach to design the controller.

In the next phase of this analysis, also the dynamic model of the finger will be included to evaluate the performance of the overall finger control. To implement the impedance control of the robotic finger, an output tendon stiffness controller will be designed.

REFERENCES

- [1] L. Biagiotti, F. Lotti, C. Melchiorri, P. Tiezzi, and G. Vassura. Ubh 3: an anthropomorphic hand with simplified endo-skeletal structure and soft continuous fingerpads. In *Proc. IEEE Int. Conf. on Robotics and Automation*, 2004.
- [2] L. Biagiotti, F. Lotti, C. Melchiorri, G. Palli, P. Tiezzi, and G. Vassura. Development of ub hand 3: Early results. In *Proc. IEEE Int. Conf. on Robotics and Automation*, 2005.
- [3] F. Lotti and G. Vassura. A novel approach to mechanical design of articulated finger for robotic hands. In *Proc. IEEE/RSJ IROS Int. Conf. on Intelligent Robot and Systems*, 2002.
- [4] N. Hogan. Impedance control: An approach to manipulation, parts i-iii. *ASME Journal of Dynamic Systems, Measurement and Control*, 107:1–24, 1985.
- [5] S. Stramigoli, C. Melchiorri, and S. Andreotti. A passivity-based control scheme for robotic grasping and manipulation. In *Proc. of the 38th IEEE Conference on Decision and Control*, 1999.
- [6] M. Kaneko, T. Yamashita, and K. Tanie. Basic considerations on transmission characteristics for tendon drive robots. In *Advanced Robotics, 1991. 'Robots in Unstructured Environments', 91 ICAR, Fifth International Conference on*, pages Page(s):827 – 832 vol.1, 19–22 June 1991.
- [7] M. Kaneko, M. Wada, H. Maekawa, and K. Tanie. A new consideration on tendon-tension control system of robot hands. In *Robotics and Automation, 1991. Proceedings., 1991 IEEE International Conference on*, pages Page(s):1028 – 1033 vol.2, 9–11 April 1991.
- [8] H. Olsson, K.J. Åström, C. Canudas de Wit, M. Gäfvert, and P. Lischinsky. Friction models and friction compensation.
- [9] W. Townsend and J. Jr. Salisbury. The effect of coulomb friction and stiction on force control. In *Robotics and Automation. Proceedings. 1987 IEEE International Conference on*, volume 4, pages 883 – 889, Mar 1987.
- [10] M. Kaneko, W. Paetsch, and H. Tolle. Input-dependent stability of joint torque control of tendon-driven robot hands. In *Industrial Electronics, IEEE Transactions on*, volume 39, Issue 2, pages 96 – 104, April 1992.